

Using Data-Science Approaches to Unravel Insights for Enhanced Transport of Lithium Ions in Single-Ion Conducting Polymer Electrolytes

Qinyu Zhu, Yifan Liu, Lauren B. Shepard, Debjyoti Bhattacharya, Susan B. Sinnott, Wesley F. Reinhart, Valentino R. Cooper, and Rajeev Kumar*



Cite This: *Chem. Mater.* 2024, 36, 11934–11946



Read Online

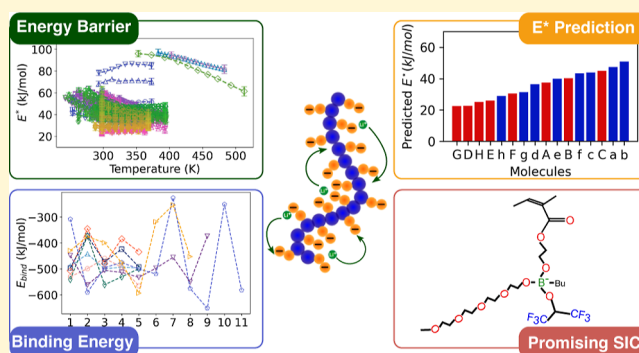
ACCESS |

Metrics & More

Article Recommendations

Supporting Information

ABSTRACT: Solid polymer electrolytes have yet to achieve the desired ionic conductivity (>1 mS/cm) near room temperature required for many applications. This target implies the need to reduce the effective energy barriers for ion transport in polymer electrolytes to around 20 kJ/mol. In this work, we combine information extracted from existing experimental results with theoretical calculations to provide insights into ion transport in single-ion conductors (SICs) with a focus on lithium ion SICs. Through the analysis of temperature-dependent ionic conductivity data obtained from the literature, we evaluate different methods of extracting energy barriers for lithium transport. The traditional Arrhenius fit to the temperature-dependent ionic conductivity data indicates that the Meyer–Neldel rule holds for SICs. However, the values of the fitting parameters remain unphysical. Our modified approach based on recent work (*Macromolecules* 2023, 56, 15, 6051), which incorporates a fixed pre-exponential factor, reveals that the energy barriers exhibit temperature dependence over a wide range of temperatures. Using this approach, we identify anions leading to the energy barriers <30 kJ/mol, which include trifluoromethane sulfonimide (TFSI), fluoromethane sulfonimide (FSI), and boron-based organic anions. In our efforts to design the next generation of anions, which can exhibit the energy barriers <20 kJ/mol, we have performed density functional theory (DFT) based calculations to connect the chemical structures of boron-based anions via the binding energy of cation (lithium)-anion pairs with the experimentally derived effective energy barriers for ion hopping. Not only have we identified a correlation between the binding energy and the energy barriers, but we also propose a strategy to design new boron-based anions by using the correlation. This combined approach involving experiments and theoretical calculations is capable of facilitating the identification of promising new anions, which can exhibit ionic conductivity >1 mS/cm near room temperature, thereby expediting the development of novel superionic single-ion conducting polymer electrolytes.



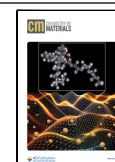
INTRODUCTION

The increasing global energy consumption and environmental apprehension associated with fossil fuels necessitate the advancement of next-generation energy storage materials. The prevalent use of flammable liquid electrolytes in current lithium-ion batteries poses considerable safety risks.^{1,2} Consequently, substantial efforts have been invested in the development of alternative electrolytes that not only enhance safety but also improve overall device performance. Solid polymer electrolytes (SPEs) have emerged as a potentially safer and more robust solution to pressing energy issues. SPEs eliminate the liquid medium common in commercial electrolytes, thereby addressing safety concerns associated with leakage and flammability.^{3–6} Moreover, the flexibility of polymer electrolytes opens up opportunities for designing and manufacturing novel devices that require energy storage systems at different scales, as polymeric materials can be

tailored to different geometries and forms to fit various applications.

Over the past decades, significant efforts have focused on improving the ionic conductivity of SPEs using various approaches, which includes modifying the morphology and crystallinity of the polymer matrix, modifying the types of salt used, adjusting the salt concentrations, adding nanostructured fillers and plasticizers, etc.^{7–12} In the pursuit of next-generation electrochemical devices, the studies of single-ion conductors

Received: August 29, 2024
 Revised: November 19, 2024
 Accepted: November 20, 2024
 Published: December 6, 2024



(SICs) have been pivotal.^{4,13} Generally, SICs consist of a mobile ion, such as Li⁺, and a polymerized counterion, offering unique properties that have the potential to overcome limitations associated with traditional electrolyte materials. For instance, while some dual ion conductors exhibit relatively high ionic conductivity, the contributions from lithium ion transport are relatively low as lithium tends to associate with the polymers, thereby restricting its mobility in the polymer matrix. Such imbalanced ion transport often leads to local depletion of lithium, which significantly diminishes the achievable capacity and cycling stability.¹⁴ While it is a concern that immobilizing anions will almost certainly lead to a decrease in ionic conductivity, single ion conductors are considered a potential solution to alleviate the concentration polarization phenomena in dual ion conductors, especially at high current densities.^{14–16} Therefore, exploring the mechanisms of ion transport can enable the design of novel SICs with enhanced conductivity, a crucial step for developing more durable energy storage applications.

The conventional principles of lithium ion-based SIC design mainly focus on two aspects: (1) disassociation between the cation and anion pairs, and (2) optimized lithium ion transport across the polymer matrix. The first design principle involves reducing electrostatic interactions between cations and anions, typically achieved by introducing electron-withdrawing functional groups near anions that delocalize negative charges.^{17,18} Using polymers with high dielectric constants has also been theoretically proven to accelerate the disassociation of the cation–anion pairs to achieve improved conductivities.^{19,20} The second strategy emphasizes facilitating lithium ion “solvation” without impeding the transport. One way to achieve this is to modify the polymer backbones to promote fast segmental dynamics, e.g., lowering the glass transition temperature (T_g).^{21,22} An alternative approach is to incorporate additives such as plasticizers or other neutral polymers to reduce the degree of crystallinity, thereby increasing the polymer segmental mobility.^{23–25} This enables the balanced dissolution and migration of lithium ion in the background polymer matrix. Another way is to promote decoupling of lithium ion transport from the polymer matrix dynamics. Meanwhile, the mobility of anions should also be constrained to ensure the maximum conductivity contribution from the cations. The most common way is to bind the anions to the polymer backbone, so that the motions of anions are highly correlated to the polymer matrix, thereby slowing down the migration of anions.^{11,13}

Despite the fruitful results obtained by following the aforementioned empirical basis, a definitive systematic conclusion regarding microscopic ion transport mechanisms remains elusive based on existing results. The conductivities of most SICs remain significantly below the target of 1 mS/cm under ambient conditions, therefore impeding the large-scale application of SICs in practical scenarios. Although a substantial amount of high-quality data is available in the literature, limited effort has been made to thoroughly extract and analyze the information, resulting in a lack of fundamental understanding of enhanced ion transport in SICs. It is intuitive to consider browsing through the experimental results in the vast literature and establishing a database that provides all the useful information for a more comprehensive and efficient data analysis. Creating such a database is indeed labor-intensive, as it relies mostly on manual extraction and requires specific expertise to assess the credibility of the information. A recent

initiative by Schauer et al. represents a commendable step forward.²⁶ They have compiled a relatively comprehensive and reliable database focusing on Li-conducting polymers, with accessible visualization tools for easy comparison among different families of molecules. This contribution stands out as a valuable resource for the polymer electrolyte community, addressing the scarcity of exhaustive databases and providing a foundation for further research in the field.

In this work, we integrate the SIC data sets from the database distributed by ref 26, along with some of the more recent experimental results, to present a comprehensive analysis of ionic conductivity data. The main purpose is to provide insights into the design rationale of SICs using ion transport energy barriers as a guiding principle. We compare the results of different methods for extracting energy barriers, including the traditional Arrhenius-type fit^{26,27} and alternative effective energy barriers that vary with temperature.²⁸ We then focus on the investigation of a specific class of boron-based single-ion lithium conducting polymers reported in the literature.²⁹ We perform density functional theory (DFT) calculations to estimate the binding energy between Li⁺ and the boron-containing anions. This allows us to relate observations at the macroscopic level to electron-scale properties. We subsequently propose a series of new boron-based SICs based on the existing ones and calculate their binding energies using DFT. We also predict the effective energy barriers of these new molecules based on the correlations obtained from the previous step. We anticipate that the data science approach used in this work can be extended to other polymer electrolyte systems, thereby expediting the design and discovery of advanced electrolyte materials for current and future technologies.

METHODS

Extracting Energy Barriers for Ion Hopping from Experimental Data. Traditionally, the energy barrier for ionic transport in glassy materials can be estimated by assuming Arrhenius behavior of the conductivity^{27,30}

$$\sigma(T) = \sigma^* \exp\left(\frac{-E_a}{k_B T}\right) \quad (1)$$

where σ^* is the pre-exponential factor, and E_a is regarded as a constant thermal activation energy barrier of ion transport near and below T_g . This method has provided fruitful analysis in the past decades but failed to interpret the conductivity data above T_g . Instead, the conductivity data above T_g are fit to other correlations, including the Vogel–Tamman–Fulcher (VTF) equation,^{31,32} the Williams–Landel–Ferry (WLF) equation,^{33,34} and other empirical equations.^{35,36} However, the fitting parameters in these phenomenological equations do not provide physical insights into the fundamental mechanism of ion transport in polymeric systems, as shown below.

Alternatively, our recent work suggests that a temperature-dependent energy barrier provides a more reasonable analysis of the conductivity data.²⁸ Instead of the conductivity relaxation time analysis presented in ref 28, here we choose to directly analyze the DC conductivity. We first write the conductivity of a SIC using the Nernst–Einstein formalism^{37–39}

$$\sigma(T) = \frac{q^2 e^2 c D H^{-1}(T)}{k_B T} \quad (2)$$

where q is the valency of the ion, e is the elementary charge, c is the concentration of the ion, D is the diffusivity of the ion, $H^{-1}(T)$ is the temperature dependent inverse Haven ratio,^{4,40} k_B is the Boltzmann constant, and T is the temperature. We can express the diffusivity

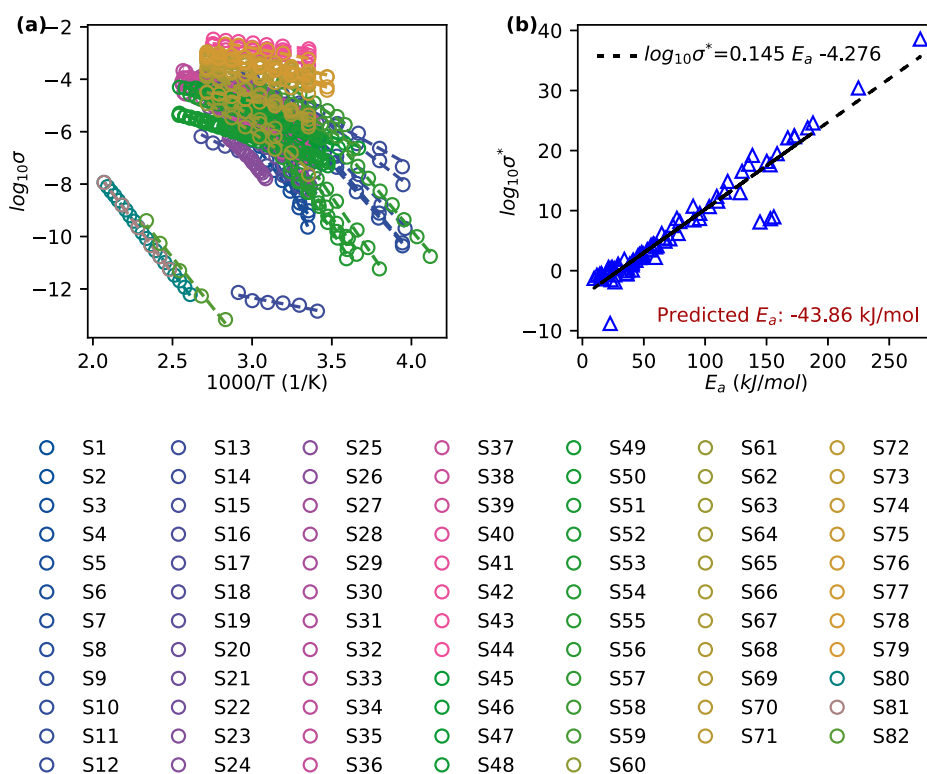


Figure 1. (a) Traditional Arrhenius fit of SIC data collected from the literature using eq 1 by taking $\ln \sigma^*$ and E_a as fit parameters. (b) Meyer–Neldel (MN) rule is shown to be valid for the fitted parameters, with an unphysical energy barrier predicted for achieving 1 mS/cm at room temperature.

using the average distance and rate of ion hopping, and augment the expression for ion diffusion over an energy barrier

$$D = \frac{d^2(T)}{6\tau(T)} \quad (3)$$

$$\tau(T) = \tau_0 \exp\left(\frac{E^*(T)}{k_B T}\right) \quad (4)$$

where $\tau(T)$ is the conductivity relaxation time, τ_0 is the characteristic conductivity relaxation time, $d(T)$ is the temperature-dependent hopping distance for ion transport, and $E^*(T)$ is the effective energy barrier that depends on temperature. We can then rewrite eq 2 as

$$\sigma(T) = \sigma_0 \left(\frac{T_0}{T}\right) \left(\frac{d(T)}{d_0}\right)^2 \exp\left(\frac{-E^*(T)}{k_B T}\right) H^{-1}(T) \quad (5)$$

where we have defined a characteristic conductivity σ_0 at a reference temperature and hopping distance of T_0 and d_0 by

$$\sigma_0 = \frac{q^2 e^2 c d_0^2}{k_B T_0 6\tau_0} \quad (6)$$

For simplicity, we assume that the hopping distance does not vary with temperature, i.e., $d(T)/d_0 = 1$, and $H^{-1}(T) = 1$. Therefore, we can rearrange eq 5 and define an effective temperature dependent energy barrier

$$E^*(T) = -k_B T \ln\left(\frac{\sigma T}{\sigma_0 T_0}\right) \quad (7)$$

With a constant parameter estimated as

$$\sigma_0 T_0 = \frac{q^2 e^2 c d_0^2}{6k_B \tau_0} = \frac{q^2 e^2 c D_0}{k_B} \quad (8)$$

To evaluate the constant prefactor, we can take T_0 to be ambient condition of 300 K. The value of D_0 can be approximated using values typical for gas diffusion through polymer membranes, ranging from 10^{-4} to 10^{-3} cm²/s.⁴¹ The concentration of ion c varies between 1 and 10 nm⁻³ depending on the size of the ion. The corresponding values for σ_0 are expected to fall within the range of 0.62–62 S/cm. We can then evaluate a reasonable range for the effective energy barriers, and we will present more detailed results and discussions below.

Density Functional Theory Calculations. In this study, we use Quantum ESPRESSO (QE) v6.3 to perform DFT calculations and evaluate the lithium binding energies.⁴² A plane wave kinetic energy cutoff of 100 Ry was consistently used, with an energy convergence threshold for self-consistency set at 10^8 Ry. GBRV PBE ultrasoft⁴³ pseudopotentials and the vdW-DF-C09⁴⁴ exchange–correlation functional were applied, with a Γ k -point grid for all simulations. The specific electron configurations used in the pseudopotentials were as follows:

- Hydrogen (H): $1s^1$
- Lithium (Li): $[\text{He}] 2s^1$
- Boron (B): $[\text{He}] 2s^2 2p^1$
- Carbon (C): $[\text{He}] 2s^2 2p^2$
- Oxygen (O): $[\text{He}] 2s^2 2p^4$
- Fluorine (F): $[\text{He}] 2s^2 2p^5$

Each anion was simulated after assigning an extra electron (a negative net charge), while the Li^+ calculation was performed with one electron removed. All computations were conducted in the gas phase within a vacuum box to eliminate interactions arising from periodic boundary conditions. We maintained a minimum separation of 16 Å between molecules to ensure complete isolation. Initial atomic configurations are generated by translating SMILES representations using the RDKit package,⁴⁵ an open-source cheminformatics toolkit.

The binding energy of an anion and lithium cation represents the energy required to separate the two ions and move them to an infinite distance apart. Mathematically, the binding energy (E_{bind}) can be expressed as

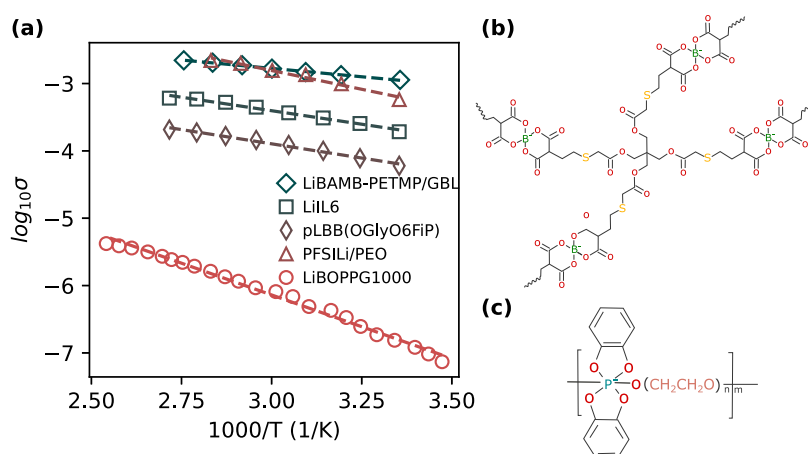


Figure 2. Selected results of Arrhenius energy barrier analysis. (a) The Arrhenius energy barriers of selected SIC with the lowest E_a , including lithium bis(allylmalonato)borate-pentaerythritol tetrakis(2-mercaptoacetate) (labeled as LiBAMB-PETMP/GBL, $E_a = 9.52$ kJ/mol),⁵² lithium borate ionic liquid (labeled as LiLi6, $E_a = 15.35$ kJ/mol),⁵³ polarizable methacrylic borate lithium salt (labeled as pLBB(OGLyO6FiP), $E_a = 16.15$ kJ/mol),²⁹ lithium poly(perfluoroalkylsulfonyl)imide/poly(ethylene oxide) blend (labeled as PFSiLi/PEO, $E_a = 21.31$ kJ/mol),⁵⁴ and lithium bis(oxalato)phosphate propylene glycol (labeled as LiBOPPG1000, $E_a = 36.11$ kJ/mol).⁵⁵ The labels are taken from the original manuscripts for easier reference. We summarize two categories of anions with one of the lowest fitted E_a : (b) boron-containing SIC LiBAMB-PETMP/GBL reported in ref S2; (c) phosphate-containing SIC LiBOPPG1000 reported in ref S5.

$$E_{\text{bind}} = E_{\text{anion-Li}} - E_{\text{anion}^-} - E_{\text{Li}^+} \quad (9)$$

where $E_{\text{anion-Li}}$ is the total energy of the combined anion and lithium cation system; E_{anion^-} is the energy of the isolated anion; E_{Li^+} is the energy of the isolated lithium cation. A comparative analysis of anion-Li binding energies using different reference systems was conducted. See Figure S1 in Supporting Information for details.

RESULTS AND DISCUSSION

Traditional Arrhenius Fit of Single-Ion Conductor

Data. As a first step, we fit the collected conductivity data to eq 1. Since the Arrhenius equation is valid near or below T_g , we choose data sets with available T_g information and only fit the data points below T_g . We also include some data sets if the sum squared errors (SSEs) of the Arrhenius fits in the low-temperature range are within a threshold value, i.e., the linear relationship between $\log(\sigma)$ and $1/T$ holds. We show in Figure 1a the Arrhenius fit for a total of 82 distinctive samples. The majority of activation energies fall between 50 and 200 kJ/mol (see the abscissa of Figure 1b), which are comparable to the reported values in the literature.

In Figure 1b, we plot the logarithm of σ^* against E_a . All of the data points fall on a single line, suggesting that the activation energy and Arrhenius prefactor for these SIC systems follow the Meyer–Neldel (MN) rule, also known as the isokinetic relationship or compensation effect.^{46,47} The MN rule postulates a linear relationship between the logarithm of the exponential prefactor σ^* and the thermal activation energy E_a

$$\log_{10}\sigma^* = aE_a + b \quad (10)$$

with a and b being fitting constants. The MN rule is expected to hold true in systems with Arrhenius-type activation energies, and has been observed in a number of single-component or blend-based polymer electrolytes.^{48,49}

We use the obtained MN correlation to predict the energy barrier that corresponds to a target conductivity at a specific temperature. Based on the fitted parameters a and b ($a = 0.145$ mol/kJ and $b = -4.276$ when we fit E_a in unit of kJ/mol and σ^* in unit of S/cm), we estimate the activation energy E_a to be –

43.86 kJ/mol when aiming for a conductivity of 1 mS/cm at 300 K. This implies that achieving such conductivity is theoretically feasible only when no energy barrier is present, which is unphysical in real systems. Our analysis also shows that the prefactors σ^* span an unexpectedly wide range of 40 orders of magnitude (see the ordinate of Figure 1b). The characteristic σ^* is directly related to ion hopping distance and relaxation time. The ion hopping distance is typically on the order of several angstroms,⁵⁰ while the relaxation time generally falls within the picosecond regime.^{28,51} Indeed, such variations in ion-conducting polymer materials cannot plausibly result in such an enormous difference in σ^* .

In addition, we highlight several SIC samples with the lowest values of E_a in Figure 2. The data sets are taken from refs 29–55. The Arrhenius plot of the SIC samples with the lowest E_a from each reference are presented in Figure 2a. We also draw the chemical structures of the boron-containing and phosphate-containing anions with low E_a in Figure 2b,c, respectively. Although the fitted E_a values range from 10 to 36 kJ/mol, the majority of ionic conductivity measurements fall well below 1 mS/cm. In particular, the phosphate-containing SIC reported in ref S5 exhibits an E_a of 36.11 kJ/mol, yet its conductivity is as low as 10^{-7} S/cm at room temperature. This observation contradicts the statement that an energy barrier around 30 kJ/mol is suitable for room-temperature applications.⁴ Therefore, the traditional Arrhenius approach of extracting a constant activation energy may be constrained and potentially misleading, and we need to seek more innovative approaches to interpret the experimental data.

Extracting Temperature-Dependent Effective Energy Barriers of Single-Ion Conductors.

An alternative way of extracting an effective energy barrier is to fix $\sigma_0 T_0$ in eq 7 to a reasonable value, thereby estimating the impact of temperature on the effective energy barrier for ion hopping. In this work, we vary $\sigma_0 T_0$ between 185.97 and 18,597 S·K/cm based on our previous estimates, and calculate the temperature-dependent energy barriers shown in Figure 3. Note that this alternative method applies to all available data sets, and is not limited to data points near T_g . We include a total of 142 samples in our

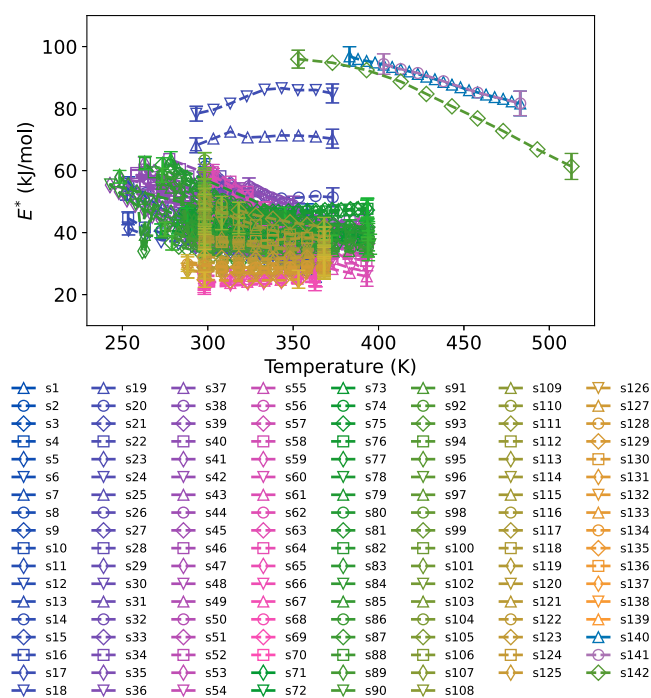


Figure 3. Temperature-dependent effective energy barriers E^* for all SIC data sets using eq 7. Note that in contrast to the restrictions in the traditional Arrhenius fit, all collected data sets are included in this analysis.

analysis. The error bars indicate the standard deviations when $\sigma_0 T_0$ changes, and we only show the variations at the lowest and highest temperatures of each sample for better visualization. For all investigated samples, E^* values appear in the range of 20–110 kJ/mol, and fluctuate by $\pm 3.01\%$ to $\pm 6.84\%$ when we sweep the values of $\sigma_0 T_0$. The values are significantly lower than the constant numbers estimated using eq 1, suggesting that the brute force Arrhenius fit could lead to potential overestimation of the energy barriers. This observation is in agreement with the conclusion of ref 28. We also estimate the energy barrier for achieving 1 mS/cm at 300 K to be 23.56 ± 2.45 kJ/mol. This estimate appears to be more reasonable and satisfies the previously reported assumption that the energy barrier should be around 20 to 30 kJ/mol for realistic applications at ambient temperature.⁴

It is worth noting that in our previous work (see ref 28), we extracted the barrier from the experimentally measured time for ionic rearrangements. In the current manuscript, we extract the energy barriers from the temperature-dependent ionic conductivity. Comparisons of the extracted barriers from the ionic conductivity and the characteristic time for ionic rearrangements for the polymers studied in ref 28 reveal virtually no difference. This comparison provides a strong-justification for extracting temperature-dependent energy barriers using the Nernst–Einstein formalism. However, in contrast to our previous work, the temperature dependence of the extracted energy barriers includes the temperature dependence of the inverse Haven ratio in addition to the material properties like the dielectric constant and the density of SIC.

We can rationalize the temperature dependency of E^* using the phenomenological Anderson and Stuart model that provides a quantitative analysis of the conduction energetics in ion-conducting media.⁵⁶ As suggested by the model, the

activation energy can be divided into (a) the electrostatic binding energy between the mobile ion and the fixed counterion site in the background media, and (b) the elastic energy required to create a large enough channel for ions to pass through. As such, the activation energy can be calculated as

$$E_a = \frac{\beta q_i q_c e^2}{\epsilon(R_i + R_c)} + 4\pi G R_i (R_i - R_D)^2 \quad (11)$$

where q_i and q_c are the valency of the mobile ion and fixed counterion, respectively, e is the elementary charge, β is the “Madelung” constant that describes the charge neutralization between the ion and its surroundings, R_i and R_c are the radii of the mobile ion and the counterion, respectively, ϵ is the dielectric constant of the medium, G is the shear modulus of the medium, and R_D is the effective radius of the preexisting doorway. The temperature dependency of the energy barrier originates from either ϵ in the Coulombic contribution or G in the elastic energy contribution. Both parameters have been experimentally proven to be temperature dependent.²⁸ The measured ϵ and G provide good estimations of E^* variations in response to temperature for selected samples, which proves the robustness of the new approach.

Figure 4a presents the effective energy barriers of selected lithium-based SIC data sets. These samples exhibit effective energy barriers less than 30 kJ/mol within the measured temperature range. The data sets are taken from refs 29, 52, 54, 57 and 58, respectively. Only the data set with the lowest effective energy barrier from each paper is included as a

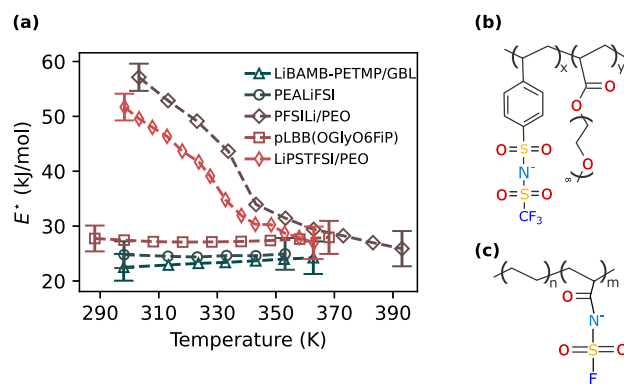


Figure 4. Selected results of extracted E^* . (a) The effective energy barriers of selected SIC samples that exhibit effective energy barriers less than 30 kJ/mol within the measured temperature range, including lithium bis(allylmalonato)borate-pentaerythritol tetrakis(2-mercaptoacetate) (labeled as LiBAMB-PETMP/GBL, $E^* = 22.50 \pm 2.44$ kJ/mol at 298 K and 24.24 ± 2.97 kJ/mol at 362 K),⁵² poly(ethylene-co-acrylic lithium (fluoro sulfonyl)imide) (labeled as PEALiFSI, $E^* = 24.79 \pm 2.44$ kJ/mol at 298 K and 24.94 ± 2.87 kJ/mol at 353 K),⁵⁷ lithium poly(perfluoroalkylsulfonyl)imide/poly(ethylene oxide) blend (labeled as PFSiLi/PEO, $E^* = 57.13 \pm 2.48$ kJ/mol at 303 K and 25.89 ± 3.21 kJ/mol at 393 K),⁵⁴ polarizable methacrylic borate lithium salt (labeled as pLBB(OGlyO₆FiP), $E^* = 27.75 \pm 2.35$ kJ/mol at 288 K and 27.95 ± 3.00 kJ/mol at 368 K),²⁹ and lithium poly[(4-styrenesulfonyl) (trifluoromethanesulfonyl)imide]/poly(ethylene oxide) blend (labeled as LiPSTFSI/PEO, $E^* = 51.69 \pm 2.43$ kJ/mol at 298 K and 26.95 ± 2.97 kJ/mol at 363 K).⁵⁸ The labels are taken from the original manuscripts for easier reference. We also identified (b) the TFSI-based SIC LiPSTFSI/PEO with the lowest E^* reported in ref 58, and (c) the FSI-based SIC PEALiFSI with the lowest E^* reported in ref 57.

representation of a class of materials. Based on the obtained effective energy barriers, the structures of the TFSI- and FSI-based anions with the lowest barriers are shown in Figure 4b,c, respectively, and the boron-based anion with the lowest E^* is still the highly cross-linked molecule reported in ref 52 (see Figure 2b).

It is noted that the temperature dependencies of E^* for boron-containing SICs (indicated by triangle and square markers in Figure 4a) are relatively weak. By contrast, for the TFSI-based SICs, the variations of E^* in temperature are more pronounced, and there are apparent transition temperatures beyond which the E^* curves become flatter. These transition temperatures generally coincide with the glass transition or crystallization temperatures, where polymer dynamics undergo significant changes. Thus, it is reasonable to hypothesize that the boron-containing molecules have a stronger decoupling between polymer and ion dynamics. Therefore, this class of materials could be a promising electrolyte candidate for the next-generation energy storage systems.

Unraveling the Origin of E^* Using Density Functional Theory Calculations. In this section, we aim to validate the relationship between binding energy, as computed by DFT-based calculations, and the effective energy barrier E^* extracted from experimental data for the purpose of designing new organic anions with enhanced ionic conductivities at room temperature. As indicated by eq 11, Coulombic interactions predominantly govern the energy barriers for small ion transport, and the elastic energy contribution becomes negligible for these smaller ions. Given our focus on the transport of small ions such as Li^+ , we hypothesize that the effective energy barrier can be derived from the binding energy obtained through theoretical calculations like DFT.

To streamline our study, we do not intend to comprehensively perform DFT calculations on all available molecules from the literature due to the prohibitive computational costs. Instead, we select a series of boron-containing molecules based on our database analysis, because they are promising candidates for next-generation SIC materials, and the monomer sizes and the number of possible binding sites of these SICs are suitable for DFT calculations within a feasible computational time frame. The extracted E^* values for these SICs are presented separately in Figure 5, with E^* ranging from 25 to 55 kJ/mol. These boron-based molecules, as referenced in ref 29, offer additional advantages due to their

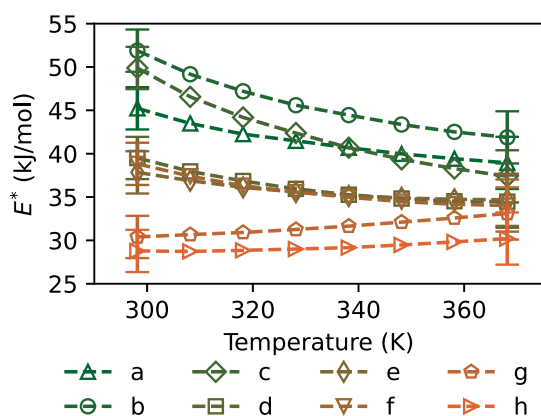


Figure 5. Extracted E^* of the boron-based SICs reported in ref 29. The molecular structures are presented later in Figure 6.

structural similarity (see Figure 6b for the molecular structures) and performance variations, allowing us to extract

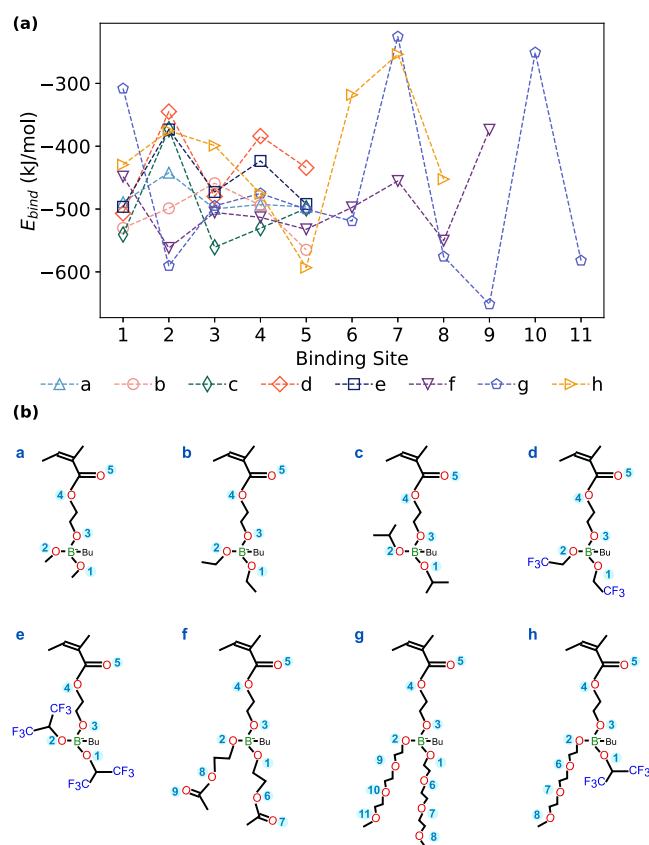


Figure 6. (a) Results of DFT binding energy calculations for the eight boron-based anions reported in ref 29, labeled as (a–h), at different preoptimization binding sites, with each indicating a unique initial configuration. The lines serve as a guide to the eye by connecting the data points of the same anion and do not reflect any trend in the change of E_{bind} . The details of binding sites and molecular structures of molecules (a–h) are presented in panel (b).

patterns from experimental data. Such a data set enables us to make connections between the chemical composition and the associated energy barrier by constructing quantitative models. Furthermore, we have designed a few novel molecules based on the existing ones with the best performance, i.e., molecules g and h presented in Figure 5. These new molecules are tailored with the following principles in mind: (1) incorporation of lithium-solvating groups to provide pathways for lithium ion conduction, (2) inclusion of electron-withdrawing groups to weaken the electrostatic interactions between lithium ions and anions, and (3) maintaining the similarity in molecular structures to the reported boron-containing molecules for further E^* prediction. We also consider the synthetic accessibility when constructing these novel molecules by accounting for possible reaction routes, the steric hindrance of the pendant groups, commercially available chemicals for synthesis, etc. The developed model based on experimental data can then be used to give reasonable estimates of E^* for these novel molecules. This strategic approach allows us to explore and identify potential improvements in the performance of this type of SIC materials.

Density Functional Theory-Based Computation of Representative Binding Energies. Due to the high

computational cost of DFT calculations, which scales cubically with the system size,⁵⁹ the boron-containing anions are represented as monomers in the binding energy calculations. Additionally, all potential binding sites are tested in the calculations. DFT-optimized structures reveal that oxygen atoms, due to their high electronegativity, typically serve as primary binding sites of lithium ions. To accurately capture the representative binding energy for each boron-based anion, individual oxygen sites are considered as starting points, and the 3D structures are generated using the RDKit package.⁴⁵ We then perform geometry optimization from each initial condition to obtain the lowest-energy configurations for binding energy calculations.

We calculated the binding energies of Li^+ with 16 boron-based anions, including the eight anions investigated experimentally in ref 29, labeled as a to h, and another eight novel SICs proposed in this work, labeled as A to H. The calculated binding energies E_{bind} are presented in Figure 6a for molecules a to h, and in Figure 7a for molecules A to H. The corresponding monomer structures and preoptimization binding sites are provided in Figures 6b and 7b, respectively.

Our results reveal substantial variations among different oxygen binding sites. However, some consistent trends are observed based on chemical structure. The strongest binding typically occurs near the three oxygen sites close to the boron atom (sites 1, 2, and 3), potentially trapping Li^+ and impeding its conduction. In contrast, two key factors contribute to

weaker binding, which accounts for the enhancement in ionic conductivity. First, SICs with more than five binding sites on the side chain exhibit weaker binding. These longer tails can potentially block strong binding sites near the boron atom, further promoting the mobility of lithium ions. This is justified in both the experimentally studied SICs (g and h) and proposed novel SICs (A, D, E, G, and H), as these SICs exhibit weaker E_{bind} , typically above -300 kJ/mol. In addition, oxygen atoms within the ethylene oxide (EO) groups play a more prominent role in reducing energy barriers compared to oxygen atoms in other functional groups like carbonyl groups, as suggested by the relatively stronger E_{bind} (~ -500 kJ/mol) in molecule f than other molecules with EO containing side chains. Second, comparisons between available SICs b and d, and novel SICs B and D, E and F, C and H, indicate that $-\text{CF}_3$ end groups on side chains tend to result in weaker E_{bind} . Thus, the presence of electron-withdrawing $-\text{CF}_3$ groups also appears to weaken binding energies.

Notably, the calculated binding energies do not quantitatively agree with the E^* extracted from the experimental data, and the values are not on the same order of magnitude. We propose the following reasons for this discrepancy. First, DFT calculations are performed at 0 K, whereas we compared the obtained binding energies to the effective energy barriers at 298 K, which is lowest temperature of the available data sets. Second, due to the high computational cost of DFT calculations, all results are obtained for binding energy between Li^+ and a negatively charged monomer structure. Thus, the effect of polymer chain length and more complex conformations cannot be easily inferred from our calculations. Last but not least, DFT calculations are performed in a vacuum, while the dielectric properties of the polymer media can be significantly different and are not taken into consideration. In fact, the values of E^* are 1 order of magnitude smaller than the absolute values of binding energies from DFT calculations, suggesting a dielectric constant around 10 of the polymeric material, which is a fairly reasonable estimation for a wide range of polymers used in SIC systems.^{60–63} Therefore, the results obtained from DFT calculations can qualitatively explain the variations in E^* due to the changes in chemical structures.

Designing New Anions by Constructing Correlations between Binding Energies and Effective Energy Barriers. For the purpose of designing new anions with superior ionic conductivity, we aim to establish a correlation between the E_{bind} derived from DFT calculations, and the E^* extracted from the experimental data. The complex energy landscape, characterized by the large fluctuation among different binding sites, necessitates a comprehensive approach to determine representative binding energies. To better capture the characteristics of the binding energies, we consider the following four key features: (1) the minimum binding energy $E_{\text{bind}}^{\text{min}}$ represents the strongest binding energy, indicating the sites where lithium ions are most likely to be trapped; (2) the maximum binding energy $E_{\text{bind}}^{\text{max}}$ denotes the weakest binding energy, suggesting the most favorable sites for lithium ion transport; (3) the mean binding energy $E_{\text{bind}}^{\text{mean}}$ reflects the average interaction strength between Li^+ and binding sites across all configurations; and (4) the sample standard deviation $E_{\text{bind}}^{\text{std}}$ quantifies the variability in binding energies, providing insight into the heterogeneity of binding sites. These features collectively characterize the potential binding scenarios within each SIC. $E_{\text{bind}}^{\text{min}}$ and $E_{\text{bind}}^{\text{max}}$ delineate the range

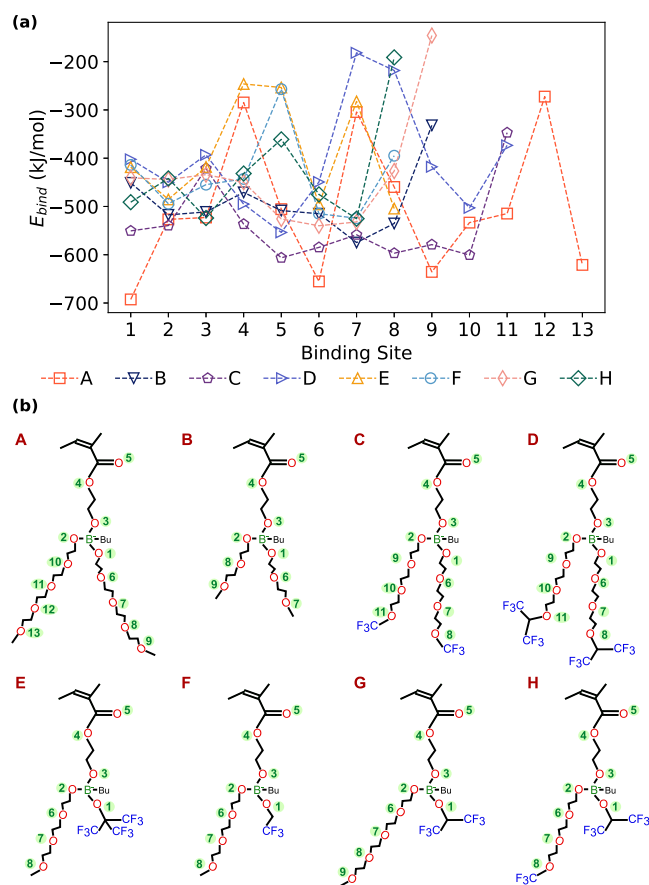


Figure 7. (a) Results of DFT binding energy calculations for the eight novel boron-based anions proposed in this study. The anions are labeled as (A–H), and the corresponding binding sites and molecular structures are shown in panel (b).

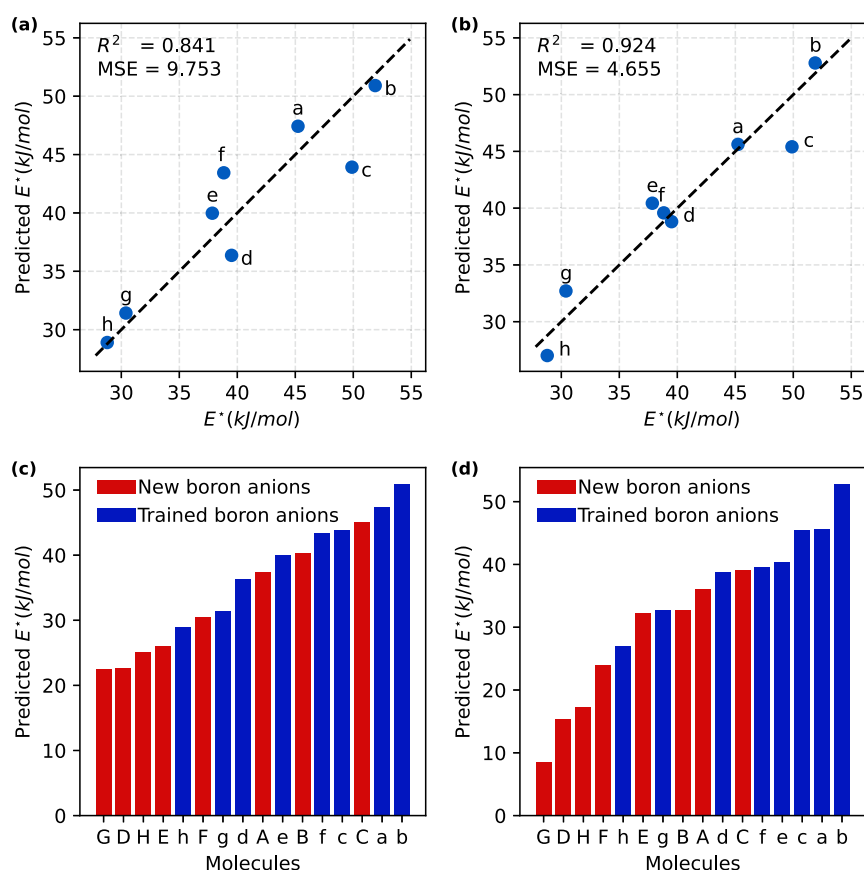


Figure 8. Comparison of two predictive models with different feature sets for SICs studied in ref 29. (a) Model trained using $E_{\text{bind}}^{\text{min}}$, $E_{\text{bind}}^{\text{max}}$, and $E_{\text{bind}}^{\text{mean}}$, with x -values showing experimental E^* and y -values indicating model-predicted barriers; (b) enhanced model incorporating $E_{\text{bind}}^{\text{std}}$ besides the previous three features; (c) predictions using the model shown in panel (a); (d) predictions using the model shown in panel (b). The red bars denote the proposed novel SICs, and blue bars represent the existing ones. The predicted E^* values for novel SICs are tabulated in Tables S1 and S2 in the Supporting Information.

of binding strengths, while $E_{\text{bind}}^{\text{mean}}$ and $E_{\text{bind}}^{\text{std}}$ offers additional information about the statistics of the calculated E_{bind} .

To explore the correlation between binding energy and effective energy barrier, we apply Lasso regression,⁶⁴ which can effectively perform feature selection when handling multiple variables, to fit models that take the aforementioned binding energy features as input and output the predicted energy barrier. The binding energy-derived features are calculated using the E_{bind} of the reported SICs (a–h), and are used for model training. The constructed models are then applied to predict the E^* for the proposed novel SICs.

Here we evaluate two different feature sets, as illustrated in Figure 8a,b. The first model, trained with $E_{\text{bind}}^{\text{min}}$, $E_{\text{bind}}^{\text{max}}$, and $E_{\text{bind}}^{\text{mean}}$ (Figure 8a), achieve a coefficient of determination (R^2) of 0.841 and a mean squared error (MSE) of 9.753, approximately 5% of the effective energy barrier. This model successfully captures the behavior of SICs with EO motifs (g and h), which exhibit the lowest energy barriers and exceptional lithium ionic conductivity. With the regularization parameter λ set to 0.5, the feature importance values for $E_{\text{bind}}^{\text{min}}$, $E_{\text{bind}}^{\text{max}}$, and $E_{\text{bind}}^{\text{mean}}$ are 0.006424, 0.073815, and 0.072500, respectively. These results highlight the importance of weak binding ($E_{\text{bind}}^{\text{max}}$) for energy barrier prediction, as indicated by the highest weight. This is closely followed by the $E_{\text{bind}}^{\text{mean}}$ input feature. $E_{\text{bind}}^{\text{mean}}$ is important because it provides a comprehensive view of the binding energy landscape, indicating whether the

overall tendency is toward weaker or stronger binding interactions.

Incorporating $E_{\text{bind}}^{\text{std}}$ as a fourth feature provides a slightly more accurate fit to the whole training set (see Figure 8b), yielding an R^2 of 0.924 and an MSE of 4.655. This model demonstrates better differentiation among various motifs: alkoxide (a, b, c), fluoroalkoxide (d, e), and additional incorporation of lithium solvating EO groups (g, h). With λ equals to 0.5, the feature importance values for $E_{\text{bind}}^{\text{min}}$, $E_{\text{bind}}^{\text{max}}$, $E_{\text{bind}}^{\text{mean}}$, and $E_{\text{bind}}^{\text{std}}$ are 0.042436, 0.244786, 0.015784, and 0.383172, respectively. These results again validate the importance of weak binding, and also highlights the importance of binding energy distribution. However, incorporating $E_{\text{bind}}^{\text{std}}$ may limit the generalizability (see Figure S2 in the Supporting Information for detailed analysis), as $E_{\text{bind}}^{\text{std}}$ is pretty sensitive to the binding site samplings.

The proposed models can then be used as a predictive tool to evaluate the proposed novel SICs. We apply both models to predict the performance of novel SICs, with results presented in Figure 8c,d. Both models consistently indicate that SICs G, D, and H are likely to exhibit low E^* , identifying them as promising candidates for excellent lithium ion conductors. These predictions are also consistent with our DFT binding energy analysis, which suggests that long molecular tails and $-\text{CF}_3$ electron-withdrawing groups are key structural features promoting efficient lithium conduction. In terms of numerical estimates, our evaluation of model performance suggests that

the first model provides more reliable predictions (see the leave-one-out cross-validation (LOOCV) results presented in the [Supporting Information](#)), as it demonstrates greater resistance to overfitting and stronger capability of generalizing across the data set to give indicative predictions. Specifically, the first model predicts an E^* of 22.44 kJ/mol for molecule G, which is considered more reasonable compared to an E^* of 8.49 kJ/mol predicted by the second model. Intuitively, this prediction is also more plausible, given the chemical and structural similarity between molecules G and h, with the latter exhibiting an experimentally extracted E^* of 28.78 kJ/mol at 298 K.

In summary, both models effectively capture the key features that affect the energy barriers, particularly in a qualitative sense. The first model demonstrates robustness, while the second model offers improved accuracy for the training data but may face challenges regarding generalizability. This analysis of combining different metrics offers a more comprehensive representation of the binding energy landscape, thereby enhancing our understanding of the complex interplay between molecular structure, binding energies, and ion transport properties for this class of boron-containing SICs. Additionally, the good agreement between our computational predictions and theoretical binding energy analysis provides a foundation for future research directions. It underscores the potential of rational molecular design in developing high-performance SICs. We anticipate that our future work will focus on validating these computational insights by synthesizing these proposed novel SICs with exceptional predicted performance. The obtained experimental data can then be used to further refine our predictive models, thereby accelerating the discovery of advanced SIC materials.

■ SUMMARY AND CONCLUSION

We have summarized and analyzed conductivity data of lithium-based SICs from the literature to provide insights into the microscopic mechanisms of ion transport and into the design rationale of SICs. While the traditional Arrhenius fit corroborates the Meyer–Neldel rule in SIC systems, the obtained fitting parameters turn out to be unphysical. We then use an alternative approach to extract temperature-dependent energy barriers with a constant pre-exponential prefactor that makes physical sense. The new approach can be used to analyze conductivity data at all temperatures. The so-estimated E^* values using physical prefactors are significantly lower than the ones calculated based on apparent Arrhenius fits, and the predicted E^* to achieve 1 mS/cm at ambient condition (~ 23 kJ/mol) is also reasonable and accessible.

In addition to identifying some of the promising anions based on our analysis, we focus on investigating a specific class of boron-containing SICs, as they demonstrate strong potential as next-generation all-solid-state polyelectrolyte materials. We perform DFT calculations to calculate the binding energies between Li^+ and the boron-containing anions, and establish a correlation between the E_{bind} and the E^* . We develop two Lasso regression models, and both effectively capture the quantitative correlations between the DFT binding energies and the E^* for the boron-based family of molecules studied in this work. While our approach to interpreting DFT data may not be the only descriptor for these boron-containing SICs, the established correlations could provide a reliable predictive model for making reasonable estimations of E^* for SICs within the same chemical family. We predict the performance of a

series of novel SICs with structures similar to those reported in the literature and identify several candidates with potential superior performance ($E^* \sim 20$ kJ/mol). Future work will focus on synthesizing and validating these promising SIC materials.

Since we have analyzed only SICs such as polymerized ionic liquids, where each monomer has a lithium ion, our conclusions for the energy barriers may not apply to dual ion conductors, where both, cations and anions, contribute significantly toward ionic conductivity. These dual ion conductors include polymers with added salt. In our recent work,⁶⁵ we have shown that transference number of cations, diffusion constant of cations and the ionic conductivity need to be analyzed in order to understand ion transport in dual ion conductors. Furthermore, microscopic descriptions of the temperature-dependent energy barriers and ionic conductivity are desired for connecting interactions among monomers, and counterions to ion transport. In addition to phenomenological models like the Anderson–Stuart model, which connects material properties like the dielectric constant to the ion transport, there is a need to describe connections between local structure and the ion transport. More sophisticated models and calculations might be necessary to account for all the effects.

It is also noted that there are several data sets for other SIC systems in our database, such as Na^+ , K^+ , Cs^+ , and Br^- conducting polymers, which are not extensively discussed in the main text.^{28,66–76} Among all the nonlithium SICs, sodium SICs are gaining attention for their potential applications in sodium-ion batteries (SIBs), as the availability of sodium reduces the dependency on limited and geographically constrained lithium resources.^{77,78} In addition, sodium-based electrode/electrolyte interfaces are less prone to forming dendrites, making SIBs perform better than lithium ion batteries in certain extreme conditions.⁷⁹ Similar to lithium SICs, sodium SICs also exhibit low ionic conductivity at ambient temperatures, usually below 10^{-6} S/cm.⁸⁰ Moreover, these materials tend to exhibit mechanical brittleness and limited electrochemical stability, particularly at high voltages and during prolonged cycling.^{81,82} The existing literature contains limited data on sodium conducting polymer systems, thus it is hard to perform a comprehensive analysis to gain mechanistic insights and optimize such materials. Nevertheless, we can strategically leverage the principles and findings from lithium SIC studies to design and develop sodium SICs with similar structural and chemical characteristics, which not only accelerates the discovery process but also helps in quickly expanding the sodium SIC database.

Moreover, there is a pressing need to develop fluorine-free SICs due to the environmental and health concerns associated with fluorinated compounds, which can produce toxic and persistent degradation products. Fluorinated functional groups benefit from strong electron-withdrawing ability that contributes to high conductivity and stability. Despite some attempts to develop nonfluorinated polyanions, the performance of these SICs either fails to meet the expectations for ambient condition applications, or does not match the effectiveness of their fluorinated analogs.^{24,29,83,84} Thus, continued research is essential to overcoming the current limitations and achieve the performance required for practical applications. One potential approach is to take advantage of artificial intelligence (AI) and large language models (LLMs), as there is an increasing trend of using AI in material discovery and development. In fact, we

have made some initial attempts to use LLM to help us predict and design novel SIC materials based on the available experimental results (see the last section in the [Supporting Information](#)). The performance of LLM is quite impressive, although more specialized training is needed to boost the feasibility and accuracy of its predictions. We expect that these AI-driven techniques will continue to evolve, thereby facilitating the exploration of previously uncharted parameter space.

Looking forward, we plan to enable public access and visualization of our database, and to continue expanding and updating the database to include data sets for more complex systems, e.g. blends of polyzwitterions and lithium salts⁸⁵ or polymer-ceramic nanocomposite,⁸⁶ in order to provide a more comprehensive perspective of the existing literature. On top of that, it is also beneficial to apply machine learning (ML) algorithms to identify some of the key features that would help improve the performance of SICs. The parameter space is vast and still largely unexplored, and it is very likely that no single feature dominates the ion hopping mechanisms in polymers. Proper application of ML to analyze large volumes of data might reveal meaningful patterns and insights that may otherwise be inaccessible. We anticipate that with a large and reliable training data set, ML models can enhance our understanding of SIC design and facilitate the discovery of new polymeric materials with improved performance.

■ ASSOCIATED CONTENT

Data Availability Statement

The data that supports the findings of this study is available at this link (<https://doi.ccs.ornl.gov/dataset/6d530ab1-ab36-55d8-bd5b-c7f71862d957>) on Constellation, a service of the Oak Ridge Leadership Computing Facility at the Oak Ridge National Laboratory, which is supported by the Office of Science of the U.S. Department of Energy under Contract no. DE-AC05-00OR22725. The repository provides access to the curated data spreadsheet with literature DOIs, DFT calculated binding energies, and scripts to analyze data, construct statistical models, and generate plots.

SI Supporting Information

The Supporting Information is available free of charge at <https://pubs.acs.org/doi/10.1021/acs.chemmater.4c02432>.

Additional results supporting the material described in this manuscript. Additional results and discussion include the comparison of DFT binding energies calculated using different reference systems, the predicted E^* values for proposed novel SICs, predictive performance comparison of the Lasso regression models, and preliminary results using LLMs ([PDF](#))

■ AUTHOR INFORMATION

Corresponding Author

Rajeev Kumar – *Center for Nanophase Materials Sciences, Oak Ridge National Laboratory, Oak Ridge, Tennessee 37831, United States*; orcid.org/0000-0001-9494-3488; Email: kumarr@ornl.gov

Authors

Qinyu Zhu – *Center for Nanophase Materials Sciences, Oak Ridge National Laboratory, Oak Ridge, Tennessee 37831, United States*; orcid.org/0000-0002-2640-2214

Yifan Liu – *Materials Sciences and Technology Division, Oak Ridge National Laboratory, Oak Ridge, Tennessee 37831, United States*; orcid.org/0000-0001-5102-0552

Lauren B. Shepard – *Department of Materials Science and Engineering, The Pennsylvania State University, State College, Pennsylvania 16802, United States*

Debjyoti Bhattacharya – *Department of Materials Science and Engineering, The Pennsylvania State University, State College, Pennsylvania 16802, United States*; orcid.org/0000-0003-3707-847X

Susan B. Sinnott – *Department of Materials Science and Engineering, The Pennsylvania State University, State College, Pennsylvania 16802, United States; Department of Chemistry, Institute for Computational and Data Sciences, and Materials Research Institute, The Pennsylvania State University, State College, Pennsylvania 16802, United States*

Wesley F. Reinhart – *Department of Materials Science and Engineering, The Pennsylvania State University, State College, Pennsylvania 16802, United States; Institute for Computational and Data Sciences, The Pennsylvania State University, State College, Pennsylvania 16802, United States*; orcid.org/0000-0001-7256-2123

Valentino R. Cooper – *Materials Sciences and Technology Division, Oak Ridge National Laboratory, Oak Ridge, Tennessee 37831, United States*; orcid.org/0000-0001-6714-4410

Complete contact information is available at:

<https://pubs.acs.org/10.1021/acs.chemmater.4c02432>

Author Contributions

Q.Z.: Methodology, Investigation, Formal analysis, Visualization, Data Curation, Writing—Original Draft, Writing—Review & Editing; Y.L.: Investigation, Formal analysis, Data Curation, Writing—Original Draft; L.B.S.: Validation, Investigation, Writing—Review & Editing; D.B.: Investigation, Data Curation; S.B.S.: Supervision, Project administration, Funding acquisition; W.F.R.: Methodology, Supervision, Writing—Review & Editing; V.R.C.: Supervision, Project administration, Funding acquisition, Writing—Review & Editing; R.K.: Conceptualization, Supervision, Methodology, Project administration, Funding acquisition, Writing—Review & Editing.

Notes

The authors declare no competing financial interest.

■ ACKNOWLEDGMENTS

This work is supported as part of the Fast and Cooperative Ion Transport in Polymer-Based Materials (FaCT), an Energy Frontier Research Center funded by the U.S. Department of Energy, Office of Science, Basic Energy Sciences at Oak Ridge National Laboratory. This research used resources of the National Energy Research Scientific Computing Center (NERSC), a Department of Energy Office of Science User Facility using NERSC award BES-ERCAPm4305. We acknowledge Dr. Peter V. Bonnesen (Center for Nanophase Materials Sciences, Oak Ridge National Laboratory) for providing meaningful insights into the chemical synthesis and design of boron-containing SICs; We also thank Dr. Markus Eisenbach (Computing and Computational Sciences Directorate, Oak Ridge National Laboratory) for his expert consultation on the development of the linear regression model. This manuscript has been authored by UT-Battelle, LLC under contract no. DE-AC05-00OR22725 with the U.S. Department of Energy.

The United States Government retains and the publisher, by accepting the article for publication, acknowledges that the United States Government retains a nonexclusive, paid-up, irrevocable, worldwide license to publish or reproduce the published form of this manuscript, or allow others to do so, for United States Government purposes. The Department of Energy will provide public access to these results of federally sponsored research in accordance with the DOE Public Access Plan (<http://energy.gov/downloads/doe-public-access-plan>).

REFERENCES

- (1) Chen, Y.; Kang, Y.; Zhao, Y.; Wang, L.; Liu, J.; Li, Y.; Liang, Z.; He, X.; Li, X.; Tavajohi, N.; Li, B. A review of lithium-ion battery safety concerns: The issues, strategies, and testing standards. *J. Energy Chem.* **2021**, *59*, 83–99.
- (2) Pushparaj, R. L.; Kumar, A. R.; Xu, G. Enhancing safety in lithium-ion batteries with additive-based liquid electrolytes: A critical review. *J. Energy Storage* **2023**, *72*, 108493.
- (3) Hallinan, D. T.; Balsara, N. P. Polymer Electrolytes. *Annu. Rev. Mater. Res.* **2013**, *43*, 503–525.
- (4) Bocharova, V.; Sokolov, A. P. Perspectives for Polymer Electrolytes: A View from Fundamentals of Ionic Conductivity. *Macromolecules* **2020**, *53*, 4141–4157.
- (5) Lin, Z.; Sheng, O.; Cai, X.; Duan, D.; Yue, K.; Nai, J.; Wang, Y.; Liu, T.; Tao, X.; Liu, Y. Solid polymer electrolytes in all-solid-state lithium metal batteries: From microstructures to properties. *J. Energy Chem.* **2023**, *81*, 358–378.
- (6) Kundu, S.; Ein-Eli, Y. A review on design considerations in polymer and polymer composite solid-state electrolytes for solid Li batteries. *J. Power Sources* **2023**, *553*, 232267.
- (7) Chintapalli, M.; Chen, X. C.; Thelen, J. L.; Teran, A. A.; Wang, X.; Garetz, B. A.; Balsara, N. P. Effect of Grain Size on the Ionic Conductivity of a Block Copolymer Electrolyte. *Macromolecules* **2014**, *47*, 5424–5431.
- (8) Zhu, Q.; Wang, X.; Miller, J. D. Advanced Nanoclay-Based Nanocomposite Solid Polymer Electrolyte for Lithium Iron Phosphate Batteries. *ACS Appl. Mater. Interfaces* **2019**, *11*, 8954–8960.
- (9) Li, S.; Zhang, S.-Q.; Shen, L.; Liu, Q.; Ma, J.-B.; Lv, W.; He, Y.-B.; Yang, Q.-H. Progress and perspective of ceramic/polymer composite solid electrolytes for lithium batteries. *Adv. Sci.* **2020**, *7*, 1903088.
- (10) Anagbaos, K. I.; Król, M.; Ruokolainen, J.; Bousquet, A.; Save, M.; Rubatat, L. Improved Solid Electrolyte Conductivity via Macromolecular Self-Assembly: From Linear to Star Comb-like P(S-co-BzMA)-b-POEGA Block Copolymers. *ACS Appl. Mater. Interfaces* **2023**, *15*, 15998–16008.
- (11) Luo, S.; Liu, X.; Gao, L.; Deng, N.; Sun, X.; Li, Y.; Zeng, Q.; Wang, H.; Cheng, B.; Kang, W. A review on modified polymer composite electrolytes for solid-state lithium batteries. *Sustain. Energy Fuels* **2022**, *6*, 5019–5044.
- (12) Lee, H. C.; Kim, M.-J.; Kim, M.-H.; Yoon, T. W.; Kim, M.-E.; Lee, H. S.; Ham, D. S.; Lee, D.; Ha, C.; Kim, Y.-J.; et al. Dual-Supporter and Dual-Salt Strategy for Solid Polymer Electrolyte with High Ionic Conductivity and Elastic Toughness. *Adv. Electron. Mater.* **2023**, *9*, 2300094.
- (13) Zhu, J.; Zhang, Z.; Zhao, S.; Westover, A. S.; Belharouk, I.; Cao, P.-F. Single-ion conducting polymer electrolytes for solid-state lithium–metal batteries: design, performance, and challenges. *Adv. Energy Mater.* **2021**, *11*, 2003836.
- (14) Diederichsen, K. M.; McShane, E. J.; McCloskey, B. D. Promising routes to a high Li⁺ transference number electrolyte for lithium ion batteries. *ACS Energy Lett.* **2017**, *2*, 2563–2575.
- (15) Liu, K.; Li, X.; Cai, J.; Yang, Z.; Chen, Z.; Key, B.; Zhang, Z.; Dzwiniel, T. L.; Liao, C. Design of high-voltage stable hybrid electrolyte with an ultrahigh Li transference number. *ACS Energy Lett.* **2021**, *6*, 1315–1323.
- (16) Stolz, L.; Hochstädt, S.; Röser, S.; Hansen, M. R.; Winter, M.; Kasnatscheew, J. Single-Ion versus Dual-Ion Conducting Electrolytes: The Relevance of Concentration Polarization in Solid-State Batteries. *ACS Appl. Mater. Interfaces* **2022**, *14*, 11559–11566.
- (17) Armand, M. B. Polymer electrolytes. *Annu. Rev. Mater. Sci.* **1986**, *16*, 245–261.
- (18) Zhang, J.; Wang, S.; Han, D.; Xiao, M.; Sun, L.; Meng, Y. Lithium (4-styrenesulfonyl)(trifluoromethanesulfonyl) imide based single-ion polymer electrolyte with superior battery performance. *Energy Storage Mater.* **2020**, *24*, 579–587.
- (19) Fu, Y.; Bocharova, V.; Ma, M.; Sokolov, A. P.; Sumpter, B. G.; Kumar, R. Effects of counterion size and backbone rigidity on the dynamics of ionic polymer melts and glasses. *Phys. Chem. Chem. Phys.* **2017**, *19*, 27442–27451.
- (20) Shen, K.-H.; Hall, L. M. Effects of ion size and dielectric constant on ion transport and transference number in polymer electrolytes. *Macromolecules* **2020**, *53*, 10086–10096.
- (21) Sun, X.-G.; Reeder, C. L.; Kerr, J. B. Synthesis and characterization of network type single ion conductors. *Macromolecules* **2004**, *37*, 2219–2227.
- (22) Li, Z.; Fu, J.; Zhou, X.; Gui, S.; Wei, L.; Yang, H.; Li, H.; Guo, X. Ionic conduction in polymer-based solid electrolytes. *Adv. Sci.* **2023**, *10*, 2201718.
- (23) Klein, R. J.; Runt, J. Plasticized single-ion polymer conductors: conductivity, local and segmental dynamics, and interaction parameters. *J. Phys. Chem. B* **2007**, *111*, 13188–13193.
- (24) Liang, S.; Choi, U. H.; Liu, W.; Runt, J.; Colby, R. H. Synthesis and lithium ion conduction of polysiloxane single-ion conductors containing novel weak-binding borates. *Chem. Mater.* **2012**, *24*, 2316–2323.
- (25) Choi, U. H.; Liang, S.; O'Reilly, M. V.; Winey, K. I.; Runt, J.; Colby, R. H. Influence of solvating plasticizer on ion conduction of polysiloxane single-ion conductors. *Macromolecules* **2014**, *47*, 3145–3153.
- (26) Schausser, N. S.; Kliegle, G. A.; Cooke, P.; Segalman, R. A.; Seshadri, R. Database Creation, Visualization, and Statistical Learning for Polymer Li⁺-Electrolyte Design. *Chem. Mater.* **2021**, *33*, 4863–4876.
- (27) Bradford, G.; Lopez, J.; Ruza, J.; Stolberg, M. A.; Osterude, R.; Johnson, J. A.; Gomez-Bombarelli, R.; Shao-Horn, Y. Chemistry-informed machine learning for polymer electrolyte discovery. *ACS Cent. Sci.* **2023**, *9*, 206–216.
- (28) Gainaru, C.; Kumar, R.; Popov, I.; Rahman, M. A.; Lehmann, M.; Stacy, E.; Bocharova, V.; Sumpter, B. G.; Saito, T.; Schweizer, K. S.; et al. Mechanisms Controlling the Energy Barrier for Ion Hopping in Polymer Electrolytes. *Macromolecules* **2023**, *56*, 6051–6059.
- (29) Guzmán-González, G.; Vauthier, S.; Alvarez-Tirado, M.; Cotte, S.; Castro, L.; Guéguen, A.; Casado, N.; Mecerreyes, D. Single-Ion Lithium Conducting Polymers with High Ionic Conductivity Based on Borate Pendant Groups. *Angew. Chem.* **2022**, *134*, No. e202114024.
- (30) Ingram, M. D. Ionic conductivity in glass. *Phys. Chem. Glas.* **1987**, *28*, 215–234.
- (31) Garca-Coln, L.; Del Castillo, L.; Goldstein, P. Theoretical basis for the Vogel-Fulcher-Tammann equation. *Phys. Rev. B* **1989**, *40*, 7040.
- (32) Aziz, S. B.; Woo, T. J.; Kadir, M.; Ahmed, H. M. A conceptual review on polymer electrolytes and ion transport models. *J. Sci.: Adv. Mater. Devices* **2018**, *3*, 1–17.
- (33) Williams, M. L.; Landel, R. F.; Ferry, J. D. The temperature dependence of relaxation mechanisms in amorphous polymers and other glass-forming liquids. *J. Am. Chem. Soc.* **1955**, *77*, 3701–3707.
- (34) Shangguan, Y.; Chen, F.; Jia, E.; Lin, Y.; Hu, J.; Zheng, Q. New insight into time-temperature correlation for polymer relaxations ranging from secondary relaxation to terminal flow: Application of a universal and developed WLF equation. *Polymers* **2017**, *9*, 567.
- (35) Fontanella, J.; Wintersgill, M.; Coughlin, C.; Mazaud, P.; Greenbaum, S. Application of the bendler–shlesinger generalization

of the Vogel equation to ion-conducting polymers. *J. Polym. Sci., Part B: Polym. Phys.* **1991**, *29*, 747–752.

(36) Fontanella, J. J.; Wintersgill, M. C.; Immel, J. J. Dynamics in propylene carbonate and propylene carbonate containing LiPF₆. *J. Chem. Phys.* **1999**, *110*, 5392–5402.

(37) France-Lanord, A.; Grossman, J. C. Correlations from ion pairing and the Nernst-Einstein equation. *Phys. Rev. Lett.* **2019**, *122*, 136001.

(38) Monroe, C. W. Ionic mobility and diffusivity. *Encyclopedia of Applied Electrochemistry*; Springer, 2014; Vol. 10, pp 1125–1130.

(39) Pang, M.-C.; Marinescu, M.; Wang, H.; Offer, G. Mechanical behaviour of inorganic solid-state batteries: can we model the ionic mobility in the electrolyte with Nernst-Einstein's relation? *Phys. Chem. Chem. Phys.* **2021**, *23*, 27159–27170.

(40) Stacy, E. W.; Gainaru, C. P.; Gobet, M.; Wojnarowska, Z.; Bocharova, V.; Greenbaum, S. G.; Sokolov, A. P. Fundamental Limitations of Ionic Conductivity in Polymerized Ionic Liquids. *Macromolecules* **2018**, *51*, 8637–8645.

(41) Krevelen, D. V.; Nijenhuis, K. T. *Their Correlation with Chemical Structure; Their Numerical Estimation and Prediction from Additive Group Contributions: Properties of Polymers*; Elsevier, 2009.

(42) Giannozzi, P.; et al. QUANTUM ESPRESSO: a modular and open-source software project for quantum simulations of materials. *J. Condens. Matter Phys.* **2009**, *21*, 395502.

(43) Garrity, K. F.; Bennett, J. W.; Rabe, K. M.; Vanderbilt, D. Pseudopotentials for high-throughput DFT calculations. *Comput. Mater. Sci.* **2014**, *81*, 446–452.

(44) Cooper, V. R. Van der Waals density functional: An appropriate exchange functional. *Phys. Rev. B* **2010**, *81*, 161104.

(45) Landrum, G. *RDKit: Open-Source Cheminformatics*, 2010. <http://www.rdkit.org>.

(46) Dyre, J. C. A phenomenological model for the Meyer-Neldel rule. *J. Phys. C: Solid State Phys.* **1986**, *19*, 5655.

(47) Yelon, A.; Movaghar, B. Microscopic explanation of the compensation (Meyer-Neldel) rule. *Phys. Rev. Lett.* **1990**, *65*, 618–620.

(48) Quartarone, E.; Mustarelli, P.; Magistris, A. PEO-based composite polymer electrolytes. *Solid State Ionics* **1998**, *110*, 1–14.

(49) Muy, S.; Bachman, J. C.; Chang, H.-H.; Giordano, L.; Maglia, F.; Lupart, S.; Lamp, P.; Zeier, W. G.; Shao-Horn, Y. Lithium Conductivity and Meyer-Neldel Rule in Li₃PO₄-Li₃VO₄-Li₄GeO₄ Lithium Superionic Conductors. *Chem. Mater.* **2018**, *30*, 5573–5582.

(50) Mabuchi, T.; Nakajima, K.; Tokumasu, T. Molecular dynamics study of ion transport in polymer electrolytes of all-solid-state Li-ion batteries. *Micromachines* **2021**, *12*, 1012.

(51) Chen, K.; Schweizer, K. S. Microscopic constitutive equation theory for the nonlinear mechanical response of polymer glasses. *Macromolecules* **2008**, *41*, 5908–5918.

(52) Deng, K.; Wang, S.; Ren, S.; Han, D.; Xiao, M.; Meng, Y. Network type sp³ boron-based single-ion conducting polymer electrolytes for lithium ion batteries. *J. Power Sources* **2017**, *360*, 98–105.

(53) Guzmán-González, G.; Alvarez-Tirado, M.; Olmedo-Martínez, J. L.; Picchio, M. L.; Casado, N.; Forsyth, M.; Mecerreyes, D. Lithium Borate Ionic Liquids as Single-Component Electrolytes for Batteries. *Adv. Energy Mater.* **2023**, *13*, 2202974.

(54) Shi, Q.; Xue, L.; Qin, D.; Du, B.; Wang, J.; Chen, L. Single ion solid-state composite electrolytes with high electrochemical stability based on a poly(perfluoroalkylsulfonyle)-imide ionene polymer. *J. Mater. Chem. A* **2014**, *2*, 15952–15957.

(55) Sun, X.-G.; Angell, C. New single ion conductors (“polyBOP” and analogs) for rechargeable lithium batteries. *Solid State Ionics* **2004**, *175*, 743–746.

(56) Anderson, O. L.; Stuart, D. A. Calculation of Activation Energy of Ionic Conductivity in Silica Glasses by Classical Methods. *J. Am. Ceram. Soc.* **1954**, *37*, 573–580.

(57) Ahmed, F.; Choi, I.; Rahman, M. M.; Jang, H.; Ryu, T.; Yoon, S.; Jin, L.; Jin, Y.; Kim, W. Remarkable conductivity of a self-healing single-ion conducting polymer electrolyte, poly(ethylene-co-acrylic

lithium (fluoro sulfonyl) imide), for all-solid-state Li-ion batteries. *ACS Appl. Mater. Interfaces* **2019**, *11*, 34930–34938.

(58) Feng, S.; Shi, D.; Liu, F.; Zheng, L.; Nie, J.; Feng, W.; Huang, X.; Armand, M.; Zhou, Z. Single lithium-ion conducting polymer electrolytes based on poly[(4-styrenesulfonyl)-(trifluoromethanesulfonyl) imide] anions. *Electrochim. Acta* **2013**, *93*, 254–263.

(59) Liu, Y.; McGuinness, E. K.; Jean, B. C.; Li, Y.; Ren, Y.; Rio, B. G. d.; Lively, R. P.; Losego, M. D.; Ramprasad, R. Vapor-Phase Infiltration of Polymer of Intrinsic Microporosity 1 (PIM-1) with Trimethylaluminum (TMA) and Water: A Combined Computational and Experimental Study. *J. Phys. Chem. B* **2022**, *126*, 5920–5930.

(60) Porter, C.; Boyd, R. A dielectric study of the effects of melting on molecular relaxation in poly(ethylene oxide) and polyoxymethylene. *Macromolecules* **1971**, *4*, 589–594.

(61) Kumar, R.; Mahalik, J. P.; Bocharova, V.; Stacy, E. W.; Gainaru, C.; Saito, T.; Gobet, M. P.; Greenbaum, S.; Sumpter, B. G.; Sokolov, A. P. A Rayleighian approach for modeling kinetics of ionic transport in polymeric media. *J. Chem. Phys.* **2017**, *146*, 064902.

(62) Serra, J.; Pinto, R.; Barbosa, J.; Correia, D.; Gonçalves, R.; Silva, M.; Lanceros-Mendez, S.; Costa, C. Ionic liquid based Fluoropolymer solid electrolytes for Lithium-ion batteries. *Sustain. Mater. Technol.* **2020**, *25*, No. e00176.

(63) Barbosa, J. C.; Pinto, R. S.; Correia, D. M.; Tubio, C. R.; Gonçalves, R.; Costa, C. M.; Lanceros-Mendez, S. Solid polymer electrolytes based on a high dielectric polymer and ionic liquids for lithium batteries. *J. Power Sources* **2023**, *585*, 233630.

(64) Tibshirani, R. Regression shrinkage and selection via the lasso. *J. R. Stat. Soc. Ser. B Stat. Method* **1996**, *58*, 267–288.

(65) Kumar, R.; Zhu, Q. Dynamic density functional theory of polymers with salt in electric fields. *J. Chem. Phys.* **2024**, *161*, 104902.

(66) Das, S.; Jana, S.; Orsagh, M.; Byś, K.; Mishra, J.; Uchman, M.; Atyam, V. Building Sodium Metal Battery with Polyisoprene-Based Air-Stable Single-Ion Gel Polymer Electrolyte. *ACS Appl. Energy Mater.* **2023**, *6*, 5113–5121.

(67) Dong, X.; Liu, X.; Li, H.; Passerini, S.; Bresser, D. Single-Ion Conducting Polymer Electrolyte for Superior Sodium-Metal Batteries. *Angew. Chem., Int. Ed.* **2023**, *62*, No. e202308699.

(68) Youcef, H. B.; Orayech, B.; Del Amo, J. M. L.; Bonilla, F.; Shanmukaraj, D.; Armand, M. Functionalized cellulose as quasi single-ion conductors in polymer electrolyte for all-solid-state Li/Na and LiS batteries. *Solid State Ionics* **2020**, *345*, 115168.

(69) Genier, F. S.; Pathreker, S.; Adebo, P. O.; Chando, P.; Hosein, I. D. Design of a Boron-Containing PTHF-Based Solid Polymer Electrolyte for Sodium-Ion Conduction with High Na⁺ Mobility and Salt Dissociation. *ACS Appl. Polym. Mater.* **2022**, *4*, 7645–7663.

(70) Pan, Q.; Li, Z.; Zhang, W.; Zeng, D.; Sun, Y.; Cheng, H. Single ion conducting sodium ion batteries enabled by a sodium ion exchanged poly(bis(4-carbonyl benzene sulfonyl)imide-co-2,5-diaminobenzenesulfonic acid) polymer electrolyte. *Solid State Ionics* **2017**, *300*, 60–66.

(71) Olmedo-Martínez, J. L.; Fdz De Anastro, A.; Martínez-Ibañez, M.; Müller, A. J.; Mecerreyes, D. Polyethylene Oxide/Sodium Sulfonamide Polymethacrylate Blends as Highly Conducting Single-Ion Solid Polymer Electrolytes. *Energy Fuels* **2023**, *37*, 5519–5529.

(72) Wang, P.; Zhang, H.; Chai, J.; Liu, T.; Hu, R.; Zhang, Z.; Li, G.; Cui, G. A novel single-ion conducting gel polymer electrolyte based on polymeric sodium tartaric acid borate for elevated-temperature sodium metal batteries. *Solid State Ionics* **2019**, *337*, 140–146.

(73) Liu, K.; Xie, Y.; Yang, Z.; Kim, H.-K.; Dzwiniel, T. L.; Yang, J.; Xiong, H.; Liao, C. Design of a Single-Ion Conducting Polymer Electrolyte for Sodium-Ion Batteries. *J. Electrochem. Soc.* **2021**, *168*, 120543.

(74) Wunder, C.; Lai, T.-L.; Šiće, E.; Gutmann, T.; De Vito, E.; Buntkowsky, G.; Zarrabeitia, M.; Passerini, S. Sodium 4-styrenesulfonyl (trifluoromethanesulfonyl) imide-based Single-Ion Conducting Polymer Electrolyte Incorporating Molecular Transporters for Quasi-Solid-State Sodium Batteries. *J. Mater. Chem. A* **2024**, *12*, 20935–20946.

(75) Zhang, J.; Wang, Y.; Xia, Q.; Li, X.; Liu, B.; Hu, T.; Tebyetekerwa, M.; Hu, S.; Knibbe, R.; Chou, S. Confining Polymer Electrolyte in MOF for Safe and High-Performance All-Solid-State Sodium Metal Batteries. *Angew. Chem.* **2024**, *136*, No. e202318822.

(76) Bostwick, J. E.; Yu, D.; Zanelotti, C. J.; Dingemans, T. J.; Madsen, L. A.; Colby, R. H. High-Modulus Single-Ion-Conducting Electrolytes Based on a Rigid-Rod Polyanion. *ACS Appl. Energy Mater.* **2023**, *6*, 6910–6916.

(77) Xu, Z.; Wang, J. Toward emerging sodium-based energy storage technologies: from performance to sustainability. *Adv. Energy Mater.* **2022**, *12*, 2201692.

(78) Wickerts, S.; Arvidsson, R.; Nordelöf, A.; Svanström, M.; Johansson, P. Prospective life cycle assessment of sodium-ion batteries made from abundant elements. *J. Ind. Ecol.* **2024**, *28*, 116–129.

(79) Yadav, P.; Patrike, A.; Wasnik, K.; Shelke, V.; Shelke, M. Strategies and practical approaches for stable and high energy density sodium-ion battery: a step closer to commercialization. *Mater. Today Sustain.* **2023**, *22*, 100385.

(80) Ford, H. O.; Cui, C.; Schaefer, J. L. Comparison of single-ion conducting polymer gel electrolytes for sodium, potassium, and calcium batteries: influence of polymer chemistry, cation identity, charge density, and solvent on conductivity. *Batteries* **2020**, *6*, 11.

(81) Gebert, F.; Knott, J.; Gorkin III, R.; Chou, S.-L.; Dou, S.-X. Polymer electrolytes for sodium-ion batteries. *Energy Storage Mater.* **2021**, *36*, 10–30.

(82) Zheng, J.; Li, W.; Liu, X.; Zhang, J.; Feng, X.; Chen, W. Progress in gel polymer electrolytes for sodium-ion batteries. *Energy Environ. Mater.* **2023**, *6*, No. e12422.

(83) Martinez-Ibañez, M.; Sanchez-Diez, E.; Qiao, L.; Meabe, L.; Santiago, A.; Zhu, H.; O'Dell, L. A.; Carrasco, J.; Forsyth, M.; Armand, M.; et al. Weakly Coordinating Fluorine-Free Polysalt for Single Lithium-Ion Conductive Solid Polymer Electrolytes. *Batteries Supercaps* **2020**, *3*, 738–746.

(84) Zhu, Y.; Gao, X.; Wang, X.; Hou, Y.; Liu, L.; Wu, Y. A single-ion polymer electrolyte based on boronate for lithium ion batteries. *Electrochem. Commun.* **2012**, *22*, 29–32.

(85) Jones, S. D.; Nguyen, H.; Richardson, P. M.; Chen, Y.-Q.; Wyckoff, K. E.; Hawker, C. J.; Clément, R. J.; Fredrickson, G. H.; Segalman, R. A. Design of polymeric zwitterionic solid electrolytes with superionic lithium transport. *ACS Cent. Sci.* **2022**, *8*, 169–175.

(86) Ock, J.; Bhattacharya, A.; Wang, T.; Gainaru, C.; Wang, Y.; Browning, K. L.; Lehmann, M.; Rahman, M. A.; Chi, M.; Wang, F.; et al. Percolating Interfacial Layers Enhance Conductivity in Polymer–Composite Electrolytes. *Macromolecules* **2024**, *57*, 7489–7498.